Formation of collimated beams behind the woodpile photonic crystal

J. Trull,[1] L. Maigyte,[1] V. Mizeikis,[2] M. Malinauskas,[3] S. Juodkazis,[4] C. Cojocaru,[1] M. Rutkauskas,[3] M. Peckus,[3] V. Sirutkaitis,[3] and K. Staliunas[1,5]

[1]*Departament de Física i Enginyeria Nuclear, Universitat Politècnica de Catalunya, Colom 11, E-08222 Terrassa, Barcelona, Spain*
[2]*Division of Global Research Leaders (Research Institute of Electronics), Shizuoka University, 3-5-1 Johoku,
Naka-ku, Hamamatsu 432-8561, Japan*
[3]*Laser Research Center, Department of Quantum Electronics, Vilnius University, Sauletekio al 10, LT-10222 Vilnius, Lithuania*
[4]*Swinburne University of Technology, Centre for Micro-Photonics, John Street, Hawthorn, VIC 3122, Australia*
[5]*Institució Catalana de Recerca i Estudis Avançats (ICREA), Passeig Lluis Companys, 23, E-08010, Barcelona, Spain*

We experimentally observe formation of narrow laser beams behind the woodpile photonic crystal, when the beam remains well collimated in free propagation behind the crystal. We show that the collimation depends on the input laser beam's focusing conditions, and we interpret theoretically the observed effect by calculating the spatial dispersion of propagation eigenmodes and by numerical simulation of paraxial propagation model.

I. INTRODUCTION

Photonic crystals (PhCs) are materials with periodic modulation of the refractive index on a wavelength scale. The periodicity leads to important modifications of propagation properties of electromagnetic waves in the PhC. The modification of *temporal* dispersion, which leads to the formation of photonic band gaps in the *frequency* domain (see, e.g., [1,2] for the photonic band gaps), is well known and widely exploited. Temporal dispersion is the dependence of the frequency of propagation eigenmodes (Bloch modes) on the modulus of propagation wave number $\omega = \omega(|\vec{k}|)$. More recently it has been discovered that *spatial* dispersion can be also modified in the PhCs, allowing the control and management of the *spatial* beam propagation. The latter phenomenon can be interpreted in terms of spatial dispersion diagrams, given by the curves of constant frequency of the Bloch modes in the $\vec{k}$ space [i.e., $\omega(|\vec{k}|) = \text{const}$] or, equivalently, by $k_{||}(k_{\perp})$. The peculiarities of spatial dispersion offer new possibilities of controlling the propagation of the optical beams. Especially attractive is a suppression of diffractive broadening of the beam (or self-collimation [3–8]), which is related to the formation of flat segments in the spatial dispersion curves. One can also obtain negative refraction or super-refraction of light [9–12] when strongly tilted segments of the dispersion curves come into play. Most experimental studies of beam propagation effects in PhCs (e.g., self-collimation) are performed in two-dimensional (2D) PhCs, which are easier to fabricate experimentally. The full control over the beam propagation can be achieved in three-dimensional (3D) PhCs only. Investigations of self-collimation in 3D PhCs have been reported [13,14], but technological difficulties of fabricating finely patterned 3D materials slow down the studies. An alternative to explore the self-collimation and other beam propagation effects in 3D modulated structures is to work at microwave frequencies [15] and also in the field of acoustics (with sonic crystals) [16], where high resolution of fabrication is not required and 3D structures can be prepared by mechanical machining.

The spatial propagation effects listed above refer to the propagation of the beams *inside* the PhCs. Less is understood about how the beams behave *behind* the crystal

with nontrivial dispersion properties. It is evident that a narrow, self-collimated beam in a PhC can broaden rapidly in propagation behind the crystal. The character of the beam propagation behind the PhC depends on the wave front of the self-collimated beam. In particular, if the wave front of the beam acquires positive curvature (due to propagation in a material with negative or anomalous diffraction), then the beams can be focalized behind the modulated media [17]. The effect is related to superlensing (see [18] for theory and [19] for experiments in 2D PhCs, resulting in imaging of point sources by a PhC slice). In this way, the issues of the light propagation effects behind the PhCs deserve careful and consistent study, both to understand the physics of the waves and beam propagation in and behind the modulated materials as well as for the applications where the shaping of the beams is required. In this paper, we report an experimental observation of a well-collimated beam formation *behind* a 3D PhC of the woodpile type. We also theoretically interpret the results by expansions in plane wave components and by numerical study based on the paraxial wave propagation model in modulated media.

The article is organized as follows. First, we describe the PhC samples and report the experimental observation of beam formation by these samples. Then, we develop interpretation of the experimental observations of formation of well-collimated beams by positively curved spatial dispersion curves and surfaces of the Bloch modes in the PhC. Finally, we qualitatively reproduce the experimental observations by paraxial calculations of light propagation inside and behind the PhC structure.

II. EXPERIMENT

We used the photopolymer PhC of the woodpile type, as shown in Fig. 1. The woodpile PhC was first fabricated in Ref. [20], and this fabrication was subsequently performed by the femtosecond laser direct writing technique [21–24]. The photopolymer, in our case, was a hybrid organic-inorganic Zr containing SZ2080, ensuring high resolution and low geometrical distortions [25]. We used two types of samples: (i) moderate-contrast refractive index sample, where the
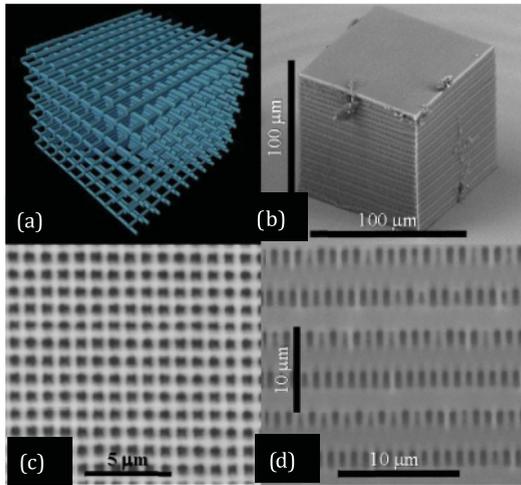
FIG. 1. (Color online) The woodpile PhC sample. Every second layer of piles of the same orientation is half-period shifted: (a) illustration and (b)–(d) micrographs by an electronic microscope showing the top (c) and side (d) views.

index varies from 1.5 in polymer to 1 in air voids, and (ii) low-contrast sample, where the voids were filled by another polymer (polyethylene glycol) diacrylate (average $M_n \sim 258$) with the refractive index of 1.45. The transverse period was 1 μm in all samples; the longitudinal periods were 9 and 8 μm for the low- and moderate-contrast samples respectively, resulting in approximately the same optical length for both kinds of samples. The PhCs contain 12 longitudinal periods (i.e., consist of 48 woodpile layers on a glass substrate) and have transverse dimensions of 80 μm [26]. The longitudinal modulation period is around one decade larger than the half-wavelength; therefore the corresponding propagation band is of a very high order (10^3 in this 3D case). We work, in this way, around a corner of a high-order Brillouin zone.

The experimental scheme and the reported experimental observation are illustrated in Fig. 2: a Continuous wave laser beam at 532 nm is focused by a ×10 objective lens to a beam waist w_o of 2 μm, and the woodpile PhC is positioned at some distance (on the order of millimeters) behind the focal plane. The PhC scatters the light, and therefore a shadow of the PhC contours is visible. At the middle of the shadow, a relatively round spot was observed, which is the key result reported in the present paper. The shape and the intensity of the spot depend on the distance between the focal plane and the crystal but do not depend on the distance to the observation plane. The remote screen, or camera located at approximately 5 cm behind the PhC, record the far-field distributions. When the spot (i.e., the well-collimated beam) is obtained, the four first-order diffraction maxima appear too, as shown in Fig. 1(b). The diffraction angles (34 and 31 deg between the central and the first maxima for moderate- and low-contrast samples, respectively) fit well with those calculated from the transverse period of the PhC (considering that the diffracted radiation leaves the crystal through the lateral facets).

The quantitative results of observation for both types of samples are summarized in Fig. 3, which evidences the existence of the optimum distance between the focal plane and the PhC sample (1 mm and 4 mm for the moderate- and
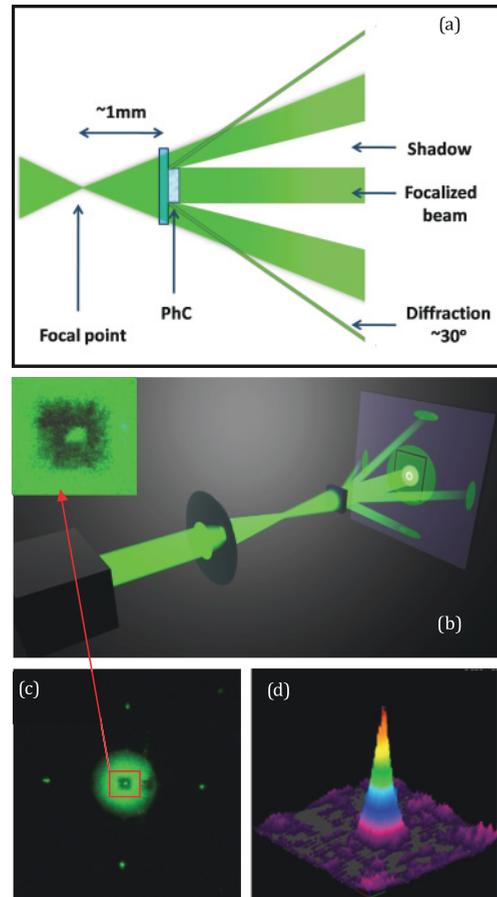
FIG. 2. (Color online) (a) The experiment to observe formation of well-collimated beam. The laser beam (532 nm) is focused (with a ×10 microscope objective), and the woodpile-like PhC is positioned at some distance (on order of millimeters) behind the focal plane. Behind the crystal, in the far-field area, the "shadow" of the PhC sample occurs, at the middle of which a narrow spot is observed, indicating formation of a well-collimated beam. (b), (c) The snapshots of typical observed transmitted field distribution on large (c) and small (d) spatial scales. The shown domain in (d) corresponds to the "shadow" of the PhC.

low-contrast samples, respectively) for the optimum beam collimation. The top intensities of the spot significantly exceeded the irradiation intensity (by approximately 4 and 14 times for the moderate- and low-contrast samples). The width of the beam was 0,12 and 0.2 relative to the width of the shadow of the sample for the moderate- and low-contrast samples, respectively, and did not depend on the distance between the PhC and the screen. This means that approximately 2% and 22% of the shadowed radiation are transferred to the well-collimated beam in moderate- and low-contrast samples, respectively.

An important observation was that the bright spot remains at the middle of the shadow by slightly tilting the PhC sample (within approximately 2 deg). This excludes all possible interpretations of the effect by the reflections from the surfaces of the sample or by a light guiding along the lateral facets or possible defect lines along the PhC.
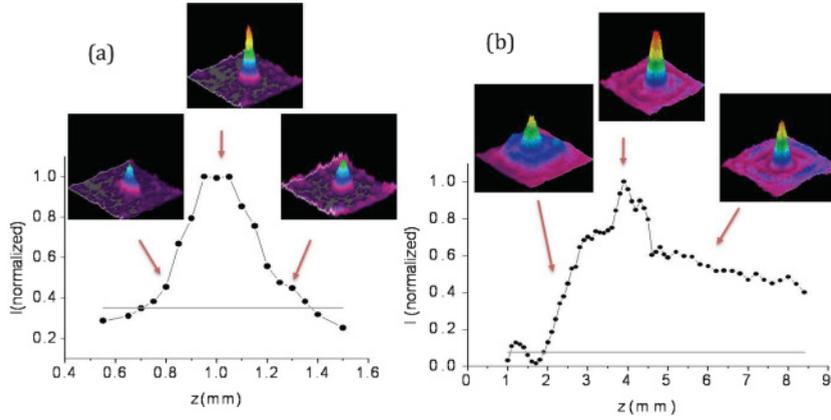
FIG. 3. (Color online) Top intensity of the collimated beam depending on the distance between the focal plane and the PhC for moderate-contrast (a) and low-contrast (b) sample. Insets show typical shapes of the beam for different positions of the PhC. Thin horizontal lines mark the intensity of the light without the crystal. The shown domains in the inset corresponds to the "shadow" of the PhC.

III. INTERPRETATION

Although the observed picture seems to be reminiscent of geometrical lensing, the observations cannot be interpreted by the ray optics: Optical thickness of the used PhC samples is constant over their transverse size; therefore the geometrical lensing due to the spherically varying thickness of the sample is excluded. Moreover, the width of the collimated beam is almost independent of the distance between PhC and the focal plane, which would not be the case for geometrical lensing. The character of collimation does not depend on the lateral dimensions of the PhC sample [26]. Also, the beam propagates in a well collimated fashion over long distances behind the PhC samples and does not exhibit a sharp focus along its path.

We interpret the beam focalization by a negative diffraction (anomalous spatial dispersion) of the Bloch modes in the bulk of the PhC. The beam front acquires a positive curvature of the wave front (due to normal spatial dispersion) in the propagation before the PhC, and the anomalous spatial dispersion inside the PhC compensates for it. The wave front of the beam therefore becomes flat or nearly flat at the back face of the PhC, which results in a well-collimated propagation behind the PhC. In order to support this interpretation, we calculate the spatial dispersion curves and surfaces evidencing the anomalous spatial dispersion and also calculate straightforwardly the light propagation in the experimental configuration.

A. Model

We use the paraxial propagation model:

$$[2ik_0\partial/\partial z + \nabla_\perp^2 + 2\Delta n(x,y,z)k_0^2]A(x,y,z) = 0. \quad (1)$$

Here $A(x,y,z)$ is the complex envelope of the electromagnetic field $E(x,y,z,t) = A(x,y,z)e^{ik_0z - i\omega_0 t}$ + c.c. propagating along the z direction with the wave number $k_0 = n\omega_0 c$ and $\nabla_\perp = \partial^2/\partial x^2 + \partial^2/\partial y^2$ is the Laplace operator in the transverse to propagation space. Relatively large spatial periods of the index variation (compared with the wavelength) justifies (1) as an acceptable approximation.

We note that the woodpile architecture allows reduction of the 3D paraxial wave equations into two separate 2D paraxial wave equations (which is impossible for the full Maxwell equations). The profile of refraction index for the woodpile PCs can be expressed as $\Delta n(x,y,z) = \Delta n_x(x,z) + \Delta n_y(y,z)$, as the woodpile structure consists of the bars directed along

the x and y directions in alternating order. The reduced 2D index profiles are of rhombic symmetry, and light propagation is parallel to the long diagonals of the rhombs, as is evident from the side view profile of the woodpile structure [Fig. 1(d)]. Then the 3D field can be factorized in this paraxial treatment: $A(x,y,z) = A_x(x,z)A_y(y,z)$, which when inserted into (1) allows us to separate the factorized components:

$$\left(2ik_0\frac{\partial}{\partial z} + \frac{\partial^2}{\partial x_i^2} + 2\Delta n_{x_i}(x_i,z)k_0^2\right)A_{x_i}(x_i,z) = 0. \quad (2)$$

Here $x_i = x, y$. Equation (2) is used for harmonic expansion of the fields and for numerical simulation of the wave propagation inside and behind the PhC.

B. Harmonic expansion

In order to calculate the spatial dispersion curves in 2D (and eventually the dispersion surfaces in 3D), the harmonic expansion can be applied to each $(x_i = x, y)$ of factorized components:

$$A_x(x,z) = e^{ik_z z}e^{ik_x x}\left(A_0(k_x) + \sum_{m_x,m_z}A_{m_x,m_z}(k_x)e^{im_x q_x x - im_z q_z z}\right). \quad (3)$$

We consider only two most relevant harmonic components $A_{m_x,m_z}(k_x)$: $(m_x,m_z) = (-1,+1),(+1,+1)$, in addition to the zero component $A_0(k_x)$: $(m_x,m_z) = (0,0)$. This truncation is justified by experimental observations, where only four diffraction maxima (two in each, the x and y directions) are visible. Speaking differently, the above truncation to three harmonic components means that the spatial modulation of the field in the Bloch mode is harmonic (i.e., the higher modulation harmonics are irrelevant). Inserting Eq. (3) into Eq. (2) results in three coupled equations for the above field components:

$$K_z A_{m_x,m_z} = (-(K_x + m_x Q_x)^2/2 + m_z Q_z)A_{m_x,m_z}$$
$$+ \Delta n_0 f \sum_{l_x,l_z \neq m_x,m_z} A_{l_x,l_z}. \quad (4)$$

Here Δn_0 is the refraction index contrast and f is the filing factor, that is, the area of the polymer bar with respect to the area of the 2D cell (in experiment $f \approx 0.1$).
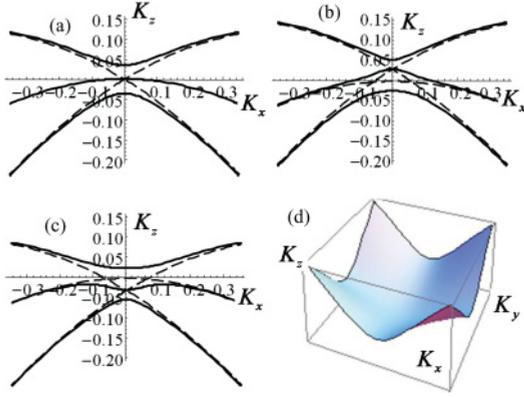
FIG. 4. (Color online) (a)–(c) Spatial dispersion curves as calculated by diagonalization of expansion (4) in 2D. (d) Spatial dispersion surface in 3D as obtained by factorization of the upper 2D spatial dispersion curve from the case (a). Parameters are $Q_x = 0.5$ and $\Delta n_0 f = 0.025$. The difference between the calculated cases is detuning from three-wave resonance (equivalently the distance from the corner of a Brillouin zone): $\Delta Q_z = (Q_z - Q_x^2/2) = 0$ for (a) and (d), $\Delta Q_z = 0.03$ for (b), and $\Delta Q_z = -0.03$ for (c). The site of square domain in plot (d) corresponds to coordinate range in (a).

$K_{x,z} = k_{x,z}/k_0$ and $Q_{x,z} = q_{x,z}/k_0$ are normalized wave vector components.

The coupling between all three harmonic components is most efficient at the resonance $Q_x^2 - 2Q_z = 0$, as follows from Eq. (4), which means that all three dispersion lines cross at $K_x = 0$ point (the dashed lines in Fig. 4). The resonance point in the paraxial model corresponds to the corner of a particular Brillouin zone in the full model. At the cross point, the lines deform due to the mode coupling and the positively curved segments appear, evidencing the negative diffraction of corresponding Bloch modes. The above resonance condition was kept in mind while fabricating the samples.

The eigenvalues of (4) have their simple analytic form expanded around the resonance point (the corner of the Brillouin zone):

$$K_z = \left[-\frac{K_x^2}{2}, \sqrt{2(\Delta n_0 f)^2 + (K_x Q_x)^2} - \frac{K_x^2}{2}, \right.$$

$$\left. -\sqrt{2(\Delta n_0 f)^2 + (K_x Q_x)^2} - \frac{K_x^2}{2} \right]. \quad (5)$$

For the formation of collimated beam, the upper branch [second eigenvalue of (5)] is important. This branch corresponds to the Bloch mode with the positive curvature (anomalous spatial dispersion). The series expansion of the corresponding branch for small k_x reads

$$K_z = \sqrt{2}(\Delta n_0 f) + \frac{K_x^2}{2}\left(\frac{\sqrt{2}}{2} \frac{Q_x^2}{\Delta n_0 f} - 1 \right) + \cdots. \quad (6)$$

This means that the PhC imposes an anomalous spatial dispersion (positive curvature) which can compensate the normal spatial dispersion (negative curvature) of the homogeneous space for $Q_x^2 \geqslant \Delta n_0 f$. Equation (6) is only the estimate of the effect, however, as it is calculated exactly at the resonance point. In reality, the curvatures of the dispersion curves of the Bloch mode depend on the detuning (i.e., on the distance from the corner of Brillouin zone), as shown in Figs. 4(a) and 4(c), and can be strongly varied by a small variation of the parameters of the PhC.

The shapes of the 3D dispersion surfaces follow straightforwardly (due to factorization) from the 2D dispersion curves calculated above and are shown in Fig. 4(d). The profile of the dispersion surface at its bottom $(K_x, K_y \to 0)$ is of high rotational symmetry, due to the parabolic character of the 2D dispersion curves in that limit. This explains a counterintuitive experimental observation that the woodpile samples, the structures of quadratic symmetry and samples of quadratic shape, form beams of a relatively high rotational symmetry.

The anomalous spatial dispersion inside the PhC plays a key role in the formation of the collimated beams: Diffractive
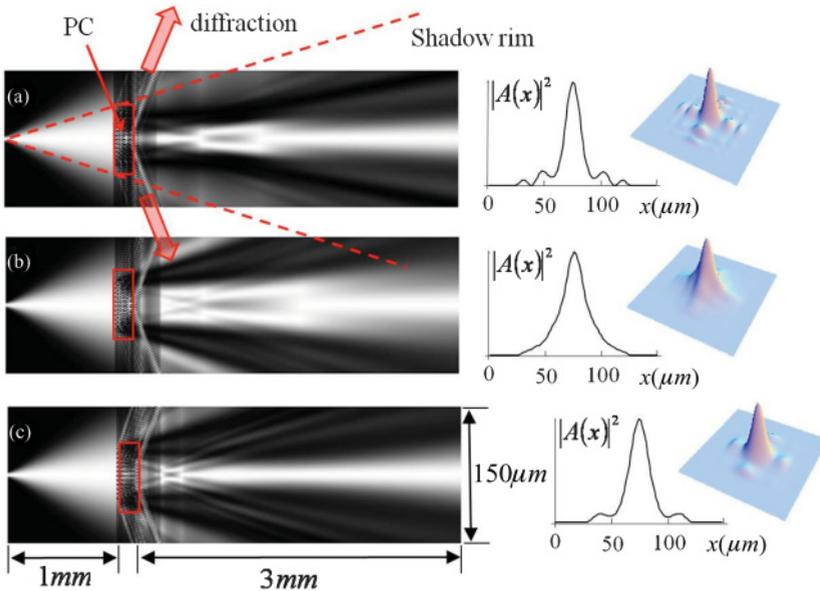
FIG. 5. (Color online) Beam propagation inside and behind the PhC as obtained by numerical integration of the paraxial model (2) in 2D. The one-dimensional (1D) profile of beam in the far-field domain and the 2D profile in the far-field domain (as obtained by factorization) are shown on the right. The site of square 2D domain corresponds to the coordinate range in 1D plots. The parameters for (a)–(c) cases correspond to these in Fig. 4.

broadening of the beam accumulated in a propagation from the focal plane to the PhC is compensated by the anomalous diffraction in propagation through the PhC. Therefore, the optimum distance between the PhC and the focal plane is determined basically by the crystal bulk parameters, that is, eventually by the curvature of the spatial dispersion curves. The curvatures of the dispersion curves of the Bloch modes depend strongly on the detuning from the corner of the Brillouin zone, as shown in Figs. 4(a)–4(c), and can be varied by fine-tuning the geometry parameters of the PhC $\Delta Q_z = (Q_z - Q_x^2/2)$. The upper branch always remains positively curved. The position of the resonance (of the corner of the Brillouin zone) depends on many parameters, including the average index of refraction. The latter depends on the thickness of the polymer bars in the samples (the filling factor), which was not precisely controllable in the fabrication of samples. Therefore, the differences among the cases in Figs. 4(a)–4(c) are beyond the fabrication precision, and we cannot definitely determine which of the these cases correspond to (both) experimentally investigated samples.

C. Numerical integration

Finally, a series of numerical simulation of the paraxial model (2) were performed in order to justify the above interpretation of the beam collimation by the dispersion curves and surfaces. Well-collimated beams in the 2D case as well as beams of relatively good rotational symmetry in 3D have been found (Fig. 5). The parameters in calculations (the size of PC sample, modulation periods) correspond to both experimental samples used, and the modulation depth ($\Delta n_0 f = 0.025$) is close to that of the estimated value of the high-contrast sample.

IV. CONCLUSIONS

We have reported experimental evidence of the formation of well-collimated optical beams from initially diverging beams by a 3D PhC at visible wavelengths. The collimation was achieved using a low-refractive-index modulation PhC structure facilitated by direct femtosecond laser writing technique. We have presented theoretical analysis which indicates that origin of the observed collimation is anomalous spatial dispersion (positively curved spatial dispersion curves in 2D and spatial dispersion surfaces in 3D). The theoretical model was validated by good qualitative agreement between the results of numerical simulations based on integration of paraxial model and the experimental data.

The collimation depends strongly on the geometric parameter $\Delta Q_z = (Q_z - Q_x^2/2)$, the normalized amplitude of index modulation $\Delta n_0 f$, and the length of the PhC structure along the beam propagation axis. It is important to achieve near-resonance condition (close to the Brillouin zone boundary) $|\Delta Q_z| \ll 1$, where collimation can occur for both negative ($\Delta Q_z < 0$) and positive ($\Delta Q_z > 0$) detuning. However, even small variations of these parameters lead to complicated and not fully understandable variation of the collimated beam quality. Better theoretical understanding and experimental optimization of the beam collimation require careful theoretical and numerical studies in the future.

Finally, it should be noted that physical mechanisms of beam formation outlined in this study are quite general and thus are applicable to a broader class of waves in periodic structures, such as acoustic waves in sonic crystals, exciton and surface polariton wave beams, and others. These principles may contribute to the development of new types of compact, misalignment-tolerant beam collimators and shapers.

[1] E. Yablonovitch, Phys. Rev. Lett. **58**, 2059 (1987).
[2] S. John, Phys. Rev. Lett. **58**, 2486 (1987).
[3] R. Zengerle, J. Mod. Opt. **34**, 1589 (1987).
[4] H. Kosaka *et al.*, Appl. Phys. Lett. **74**, 1212 (1999).
[5] R. Iliew *et al.*, Appl. Phys. Lett. **85**, 5854 (2004).
[6] D. N. Chigrin *et al.*, Opt. Express **11**, 1203 (2003).
[7] K. Staliunas and R. Herrero, Phys. Rev. E **73**, 016601 (2006).
[8] Yu. Loiko *et al.*, Opt. Commun. **269**, 128 (2007).
[9] M. Natomi, Phys. Rev. B **62**, 10696 (2000).
[10] S. Foteinopoulou and C. M. Soukoulis, Phys. Rev. B **72**, 165112 (2005).
[11] A. Lupu *et al.*, Opt. Express **14**, 2003 (2006).
[12] J. J. Baumberg *et al.*, Appl. Phys. Lett. **85**, 354 (2004).
[13] R. Iliew, C. Etrich, and F. Lederer, Opt. Express, **13**, 7076 (2005).
[14] J. Shin and S. Fan, Opt. Lett. **30**, 2397 (2005).
[15] Z. Lu *et al.*, Phys. Rev. Lett. **96**, 173902 (2006).
[16] E. Soliveres *et al.*, Appl. Phys. Lett. **94**, 164101 (2009).
[17] V. J. Sánchez-Morcillo *et al.*, Phys. Rev. B **80**, 134303 (2009).
[18] E. Cubukcu *et al.*, Phys. Rev. Lett. **91**, 207401 (2003).
[19] N. Fabre *et al.*, Phys. Rev. Lett. **101**, 073901 (2008).
[20] K. M. Ho *et al.*, Solid State Commun. **89**, 413 (1994).
[21] J. Serbin, A. Ovsianikov, and B. N. Chichkov, Opt. Express **12**, 5221 (2004).
[22] M. Deubel *et al.*, Nat. Mater. **3**, 444 (2004).
[23] V. Mizeikis *et al.*, Opt. Lett. **29**, 2061 (2004).
[24] A. Ovsianikov *et al.*, ACS Nano **2**, 2257 (2008).
[25] M. Malinauskas *et al.*, Opt. Express **18**, 10209 (2010).
[26] After submission of the paper, we performed experiments with PhCs of larger footprint, which did not bring to substantial differences.